Most reproduced "organoid-specific" cancer dependencies are consistent with culture-medium effects: a genome-wide medium-consistency audit of the 2026 organoid dependency catalogues

[AUTHORS - to be completed by submitting author]

[Affiliations]

Corresponding author: [name, email]

Abstract

Two 2026 Nature studies (Neiswender et al., Broad/NextGen; Herranz-Ors et al., Sanger) published genome-wide CRISPR dependency catalogues for patient-derived organoids, nominating organoid-specific dependencies as drug targets. Because organoid and conventional cultures differ in lipid supply, growth factors and other medium components, some dependency differences may reflect culture conditions. Neiswender et al. examined format effects genome-wide and selected medium effects using minipool and individual-gene assays. To our knowledge, catalogue-wide medium-consistency classifications and their corresponding fractions have not been reported. Here we apply prespecified medium- and format-consistency criteria to the organoid-vs-2D differential dependencies identified in our analysis of DepMap 26Q3 using organoid-medium models grown adherent (similar formulation family, no dome), dome-vs-adherent contrasts within organoid medium, and an unrelated serum-free lineage (CNS in Tumor Stem Media), with library (Avana vs Humagne-CD), lineage, and dynamic-range adjustment, on development patients with disjoint held-out-patient confirmation. Of 456 differential dependencies, 84-86% are classified medium-consistent under stated rules (75-82% under heteroscedasticity-robust SEs; bootstrap slope for adherent reproduction 0.90, 95% CI 0.82-0.99); one gene (LSM7) meets symmetric nominal criteria for format association and none do at 5% FDR. Among the Broad catalogue's published gains, 47% are medium-consistent overall and 87% of those that replicate under lineage adjustment; of Herranz-Ors et al.'s 18 headline genes, 8 of 16 present replicate - 5 medium-consistent (MVD, IDI1, MBTPS1 and MBTPS2 in the SREBP/sterol axis, plus PNKP) and 3 unresolved. Dependency losses behave similarly (84% medium-consistent); a relative ribosomal weakening survives global corrections in both assays - depletion kinetics under fewer doublings is a testable, unproven explanation. These are consistency classifications, not causal proof (adherent comparators: 6 of 9 lineages, mixed formulations). We release the per-gene table, with bootstrap flag frequencies, so any nominated organoid target can be checked before wet-lab investment.

Introduction

Organoid dependency maps are being used to nominate targets that 2D screens miss. Comparisons with conventional cell lines can confound growth format, medium, model derivation and CRISPR library; these factors differ between the two catalogues (and from classical DepMap screens). Tumour nutrient and niche-factor availability differs from culture conditions, and organoid formulations vary in their supply of extracellular lipids and signalling factors. A dependency that exists only because the medium lacks LDL may not hold in vivo; add-back experiments can test LDL limitation in cultured models, while transfer to tumors would remain untested.

What is already established, and not claimed here: Neiswender et al. (Nature 2026) used a minipool design varying growth format and culture medium, showed medium-driven sterol dependencies

(SQLE in the minipool; SQLE/MSMO1 in individual-gene assays), identified seven format-associated genes including the integrins ITGB1/ITGAV/ITGA3, and concluded format has at most modest effects under serum-free conditions; the LDLR/SREBP sterol-starvation response is textbook physiology; Wnt-secretion dependency in Wnt-free formulations is expected. Medium-associated dependencies have also been quantified at scale in cell lines (Lagziel et al. 2019; Joly et al. 2021), medium-associated components are corrected in integrated dependency resources (Pacini et al. 2021; Sanger processing documentation), screen-duration effects on late-depleting essentials are long documented (Dempster et al. 2019), a 2025 conference report describes genome-scale serum-free screens in CNS tumour models (Liang et al. 2025), and a recent commentary raises the culture-condition question for these catalogues (Zaidi & Sawyers 2026). Building on those precedents, we systematically audit the two 2026 catalogues; these observational classifications do not causally partition medium and format effects. To our knowledge, the published catalogues have not received a systematic per-gene medium-consistency audit quantifying the proportions of nominated dependency gains and losses reproduced in adherent organoid-medium models. The contribution is the systematic catalogue audit; our format-associated findings (one genome-wide candidate, LSM7, and a format-leaning unresolved set including ITGB1) are concordant with the earlier minipool analyses.

Results

Design

From DepMap 26Q3 CRISPR screens passing QC we formed, on development patients (a patient-level hold-out sequestered before analysis; calibration, gene filtering, and imputation use development screens only): organoid-medium dome models (n=68) and organoid-medium adherent models (n=9) across 9 lineages; FBS-adherent models in the same lineages (n=207); and CNS models in serum-free Tumor Stem Media vs FBS (n=29 vs 60). Per-gene library bias was removed using 22 development FBS models screened with both Avana and Humagne-CD (all Avana screens in this release are FBS, so no cross-medium invariance of the offset is assumed; transfer across FBS models is). For each gene we estimate four lineage-adjusted contrasts: D (dome organoid medium vs FBS 2D), A (adherent organoid medium vs FBS 2D - formulation family without dome; individual formulations differ), F (dome vs adherent within organoid medium), and S (TSM vs FBS in CNS). Hits (D q<0.01, |Delta-|>=0.25) are flagged medium-consistent (column medium_attributable in the released table) when A reproduces >=50% of D with nominal p<0.05 and a 90% ratio CI excluding 0, and F does not meet the symmetric criteria; format_candidate under the corresponding rule for F (same ratio/CI/nominal-p requirements, plus adherent ratio < 0.25 so the effect is not substantially reproduced without the dome); otherwise unresolved. A strict variant requiring genome-wide F q<0.05 is released alongside (flag_fdr). Flags are consistency classifications under these rules, not causal identification: the adherent comparators span 6 of 9 lineages and several formulations, and derivation/selection differences between model populations cannot be excluded by lineage adjustment. Analyses on raw Chronos and dynamic-range-normalized scores agree; normalized is primary.

Most differential dependencies are medium-consistent, in both directions

We find 249 dependency gains and 207 losses. 86% of gains and 84% of losses are medium-consistent; one gene (LSM7) is a format candidate under symmetric nominal criteria and none at 5% FDR (minimum F q ~ 1.0, so the FDR statement is about detection power, not absence of format biology - 34 hits have same-direction F/D >= 0.5). Slopes of A on D are 0.84 (gains) and 0.86 (losses), versus 0.18/0.17 for F. Under HC3 robust SEs the medium-consistent fractions are 82%/75%. Leave-one-out over the 9 adherent models: slope 0.88-0.92, >=93.5% of flags retained (F refitted per omission). A joint bootstrap (one model resample shared by calibration and analysis,

B=150; identity replicate reproduces point flags exactly) gives A-on-D slope 0.90 [95% CI 0.82-0.99]; per-gene flags are less stable than the slope (72% of hits flagged medium-consistent in >=50% of replicates; released as bootstrap frequencies), so individual flags should be read with their CIs and frequencies, not as binary truth. Restricting to the six lineages with adherent comparators (38 dome models) leaves the pattern intact (slope 0.89, median ratio 0.89, 90% of subset hits with ratio >= 0.5). Disjoint held-out patients (25 domes vs 78 reserved-patient FBS controls, no shared baseline) confirm: dev?held-out slope 0.96 (r=0.97), 100% sign concordance among medium-consistent hits, held-out adherent reproduction slope 0.90 (Fig. 1).

Named medium-consistent gains include the sterol pathway (SQLE Delta-=-0.83, adherent ratio 1.08; MSMO1 -0.81, 0.68), fatty-acid synthesis (FASN -0.42, 1.00; ACLY -0.42, 0.91), heme synthesis (ALAS1 -0.42; FECH -0.37), and Wnt secretion/reception (FZD5, LGR4, WLS; ratios 0.91-1.07, absent in TSM - consistent with Wnt-free formulations, though this conflicts with the NextGen minipool at these genes and rests on 9 adherent models).

Expression data (condition-mapped Omics TPM, same contrasts) corroborate the sterol axis on an orthogonal data type: mevalonate-pathway expression rises by median Delta- +0.36 against a dependency Delta- of -0.38 (SQLE expression +0.75 vs dependency -0.83; LDLR expression +0.61; pathway score -0.01 FBS-adherent, +0.18 organoid-medium adherent, +0.44 domes) - the expected sterol-starvation signature. Heme and fatty-acid synthesis expression move oppositely (-0.47, -0.36), so expression supports the sterol mechanism specifically (genome-wide corr(Delta-dependency, Delta-expression) ~ 0).

A specificity control comes from plasma-like medium. In Rossiter et al.'s genome-wide K562 screens (RPMI vs human plasma-like medium, both with dialyzed serum - so not an LDL-removal experiment), the HPLM-RPMI shift is genome-wide near-orthogonal to our organoid contrast (r = 0.04), and SQLE is relatively less essential in HPLM (Delta- +0.44, differential Z +3.8) versus the strongest gain in serum-free organoid medium. Genes relatively more essential in RPMI (Z>3) are enriched for our medium-consistent gains (odds ratio 4.4, prevalence ratio 4.2, Fisher p = 0.007) - medium-associated dependencies appear bidirectional and partly shared: several dependencies strongest in serum-free organoid medium are weaker in physiological than in conventional formulation in this independent system - cross-system concordance, not a shared-mechanism demonstration. (Single genome-wide line; dialyzed serum in both arms.)

Audit of the published catalogues

Against the Broad study's published organoids-vs-2D table (Mann-Whitney, unadjusted): of 285 published gains (FDR<0.05, Delta-<-0.25), 156 (55%) replicate as lineage-adjusted hits on development patients. Medium-consistent are 135 - 47% of the published list, 87% of the replicating subset - with 20 unresolved, 1 format candidate (LSM7), and 129 not reproduced under lineage adjustment (attribution unestablished, not evidence of biology). The 17 strictest gains (FDR<0.01, Delta-<-0.5) are 16 medium-consistent, 1 unresolved. Published losses (n=252): 52% medium-consistent overall, 86% of the 153 replicating.

Against Herranz-Ors et al.: their calls are prevalent within their own assay (in their BAGEL binary matrix, collapsing dual-library profiles within model, exclusive genes are depletion-called in a median 80% of organoids and headline genes in 70%; this measures call prevalence, not robustness to threshold choice, which binary calls cannot assess) - the open question is attribution. Of 97 organoid-exclusive genes (93 in the Broad table), 19 replicate as Broad differential hits (14 gains, 5 losses): 14 medium-consistent, 5 unresolved. Of the headline 18 (16 in-table), 8 replicate, all gains: 5 medium-consistent (MVD, IDI1, MBTPS1, MBTPS2, PNKP - the first four are the SREBP/sterol axis; 5/16 in-table, 5/8 of replicating) and 3 unresolved (SCAP, ratio 0.87, fails

nominal adherent significance p=0.057; DDX3X and ITGB1, ratios <=0.35). ITGB1's unresolved, format-leaning status here is consistent with Neiswender et al.'s minipool format finding for integrins.

Relative ribosomal weakening in organoid screens: depletion kinetics is a testable explanation, not an established one

The strongest individual losses are spliceosome/ribosome subunits (top Delta- up to +1.2 raw Chronos). With curated BAGEL reference sets (spliceosome n=35, ribosomal n=38), Broad median Delta- is +0.016 (spliceosome) and +0.172 (ribosomal) against +0.031 for the essential-set baseline: weakening is concentrated in subsets of subunits (13/38 ribosomal and 5/35 spliceosome genes are medium-consistent losses), with ribosomal the only complex showing a clear whole-set shift (a small hand-picked panel median reported in our earlier internal analysis, +0.90, overstates the complex-wide effect and is not used). In Broad data the shift is not a whole-screen scale change as visible after Chronos' per-screen rescaling (median common-essential Chronos ratio dome/FBS = 1.00; dome screens run longer, 24 vs 21 days), and it reproduces in adherent organoid medium (ribosomal median A +0.20, within-family format contrast -0.01) - but Chronos rescaling also means Broad data cannot speak to global dynamics directly. In Sanger's assay (organoid table 6 LFC vs 930 2D lines), reference-essential depth is 0.63x in organoids; because the two matrices are processed differently (nonessential medians also differ, -0.002 vs +0.121), we treat LFC magnitudes as secondary. On processing-robust within-model percentiles, ribosomal genes are relatively weaker in Sanger organoids (0.021 vs 0.011) while spliceosome genes are not (0.018 vs 0.027); depth-scaled LFC agrees for ribosomal (1.25 vs 1.57 xdepth). Fewer accumulated doublings with slow depletion of long-lived complexes would produce exactly this pattern, but cumulative doublings are recorded for only 1 of 1,241 Broad screens, so the mechanism is untested here and alternatives (e.g. medium-driven turnover changes) remain open. Neither 2026 catalogue reports this specific residual ribosomal pattern after its stated adjustments (Sanger does report globally fewer organoid fitness-gene calls); absolute-threshold "organoid-specific essential" calls remain exposed to it in both directions (cf. the 5 Herranz-Ors exclusives that are losses in Broad data). As a cross-system control, the mevalonate gain is visible within Sanger's assay (percentile 0.099 in organoids vs 0.394 in Sanger 2D lines).

Discussion

For target nomination the practical rule is: an organoid-specific dependency in a nutrient-synthesis pathway (sterol, fatty-acid, heme) should be prioritized for matched medium-switch and nutrient-repletion tests, because plasma supplies the end products in vivo - while noting that heme and mevalonate/GGPP dependencies can remain important in vivo (Zhu et al. 2021; Kubota et al. 2024), so pathway membership alone does not settle attribution. The sterol-axis genes on Herranz-Ors et al.'s headline list (MVD, IDI1, MBTPS1/2, SCAP) are exactly this case. Conversely, genes that do not reproduce in adherent organoid medium (DDX3X, ITGB1 among headline genes; COASY, LSM7, UTP4 among Broad published gains) are the better follow-up candidates - with ITGB1 independently format-associated in the NextGen minipool. Dependency losses deserve symmetric caution: weaker ribosomal/spliceosomal dependency in organoid screens should not be read as reduced target relevance until doublings-resolved data exist.

Limitations. (1) Identification: medium consistency is established by reproduction across different model populations sharing a formulation family; adherent comparators cover 6/9 lineages and 38/68 domes have same-lineage comparators, formulations are not identical across arms, and derivation/selection differences are not excluded. Causal medium attribution requires perturbation (add-back) experiments. (2) Uncertainty: per-gene flags are materially less stable than the aggregate slopes (bootstrap frequencies released; HC3 fractions 75-82%); the library offset rests on 22 development dual-library models, and the screen-filtered Humagne-only sensitivity has 7 FBS

controls (r=0.78 with the main estimate, slope 0.83 - consistent but inconclusive alone). (3) Format power: with 9 adherent models the F contrast detects nothing at 5% FDR; one gene passes symmetric nominal criteria. (4) Sanger analyses use published LFC tables with different processing across matrices; percentile-based results are primary. (5) CPD/doubling data are essentially absent from 26Q3, so deliverable dynamics corrections are limited to dynamic-range normalization and screen days.

Decisive tests. (1) LDL/cholesterol add-back in organoid-medium models should return the mevalonate dependency score toward the FBS baseline and restore LDLR dependency. (2) Statin/SQLE-inhibitor potency should shift >=5-fold between matched FBS and defined medium, while ITGB1-class candidates should not respond to LDL. (3) Doubling-recorded screens should test whether ribosomal Chronos recovers per doubling. A concrete protocol for (1-2) with pre-agreed falsification criteria accompanies this note.

Methods (summary)

Screens: DepMap 26Q3 ScreenGeneEffect (Chronos), ScreenSequenceMap QC filters (PassesQC, not drug-treated/engineered, in combined set), ModelCondition formulation/format annotation. Formulation classes: FBS-containing; Tumor Stem Media; organoid-defined (OPAC/organoid formulations). Patient hold-out sequestered prior to analysis (sequester_patients_v1); library offset, gene-completeness filtering, imputation, and reference sets use development screens only; held-out evaluation uses disjoint reserved-patient controls (25 domes, 5 adherent vs 78 FBS-adherent), one evaluation run. Library offset: per-gene mean Humagne-CD - Avana across 22 development dual-screened FBS models, applied to Avana (all-FBS) screens. Contrasts: per-gene OLS on model-mean Chronos with lineage dummies; t-based p, Benjamini-Hochberg q per contrast; HC3 robust SEs released and used for a flag sensitivity. Normalization: per screen, nonessential median ? 0, common-essential median ? -1 (development FBS-adherent-defined sets: 978 essentials, 5,027 nonessentials). Ratio CIs by delta method (shared-baseline covariance omitted, which widens CIs for same-sign candidates conditional on calibration; joint uncertainty is estimated by a bootstrap sharing one model resample between calibration and analysis (B=150, per-hit flag frequencies released; reference sets frozen at point estimates)). Common-support sensitivity restricts to the six lineages with adherent organoid-medium models. Humagne-only sensitivity filters screens before aggregation. Published tables: Broad figshare organoids_vs_2d_gene_dependency_tests_full.csv; Herranz-Ors supplementary table 4 (organoid_core_fitness_genes) and table 5 binary calls (collapsed within model across libraries); Sanger organoid LFC (supplementary table 6) vs cell-line EssMatrix; Rossiter et al. Table S1 gene scores (PMC8172426). Expression: Omics TPM logp1 mapped to model conditions via embedded ModelConditionID. Code: src/medium_attribution_v2.py and companions (_heldout, _loo, _boot, sanger_direct_check3.py, sanger_tables_audit.py, panels_curated.py, expression_triangulation.py, hplm_reverse_test.py); outputs under generations/medium_attribution_v2_* and release_v1/tables/.

References

1. Neiswender et al. A dependency map enhanced with next-generation 3D cancer models. Nature 2026. doi:10.1038/s41586-026-10843-7.

2. Herranz-Ors et al. A tumour-derived organoid biobank maps cancer gene dependencies. Nature 2026. doi:10.1038/s41586-026-10830-y.

3. DepMap 26Q3 release (Chronos gene effects, screen/model-condition metadata).

4. Rossiter NJ et al. CRISPR screens in physiologic medium reveal conditionally essential genes in human cells. Cell Metab. 2021;33(6):1248-1263.e9. doi:10.1016/j.cmet.2021.02.005 (PMC8172426, Table S1).

Figures

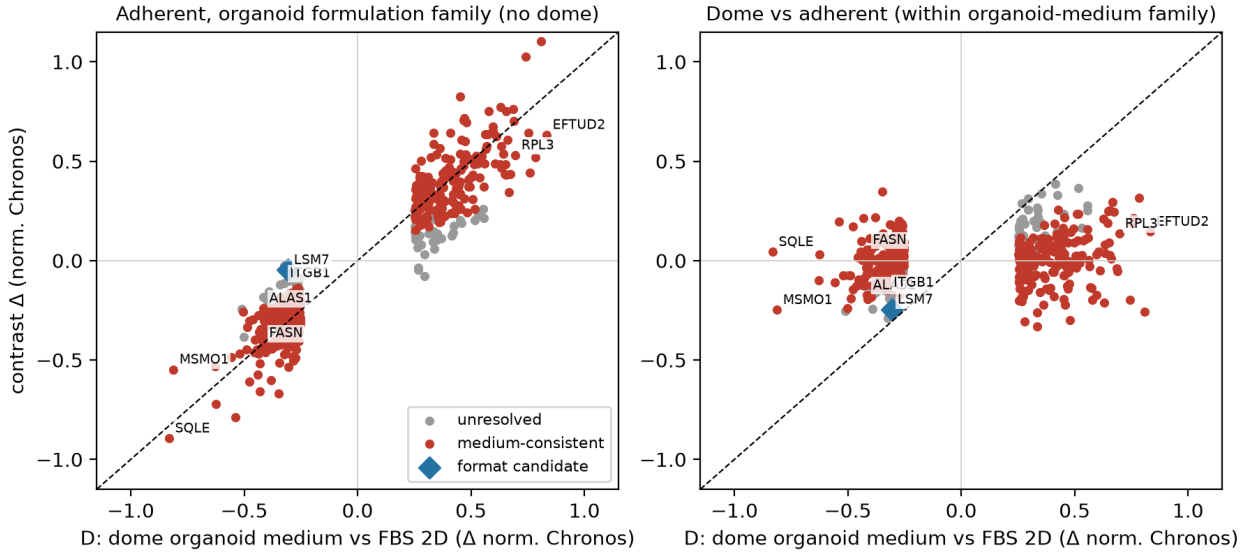


Figure 1. Attribution of organoid-vs-2D differential dependencies. Left: adherent organoid-formulation-family effect (A) vs dome effect (D). Right: dome vs adherent within the organoid-medium family (F) vs D. Dashed: identity.

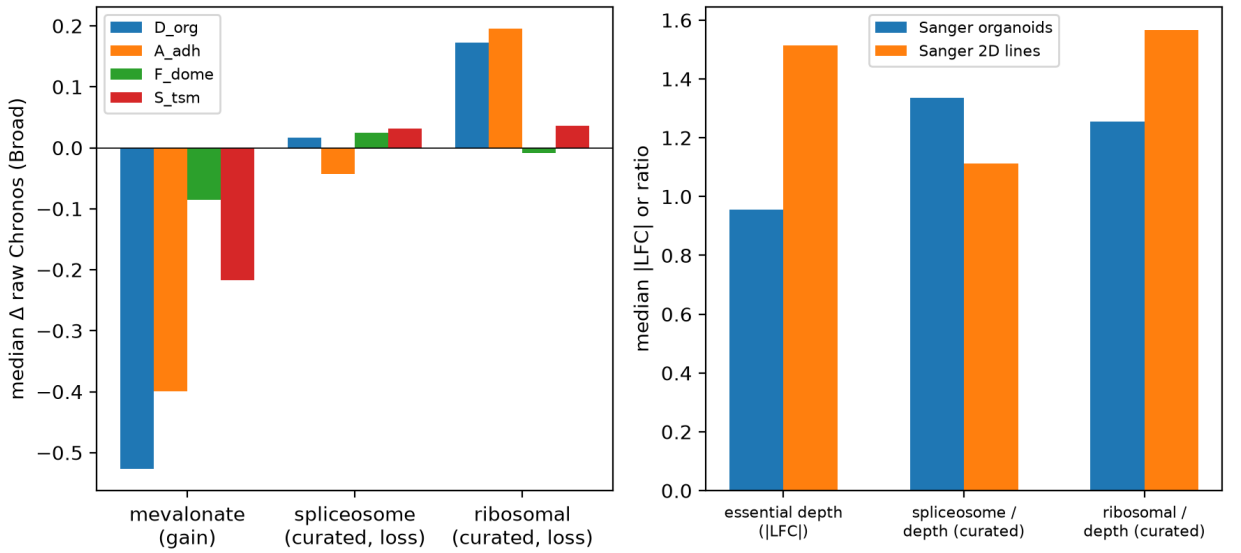


Figure 2. Core-essential weakening with curated BAGEL reference sets. Left: Broad median delta-Chronos by contrast. Right: Sanger essential depth and depth-scaled panel ratios.

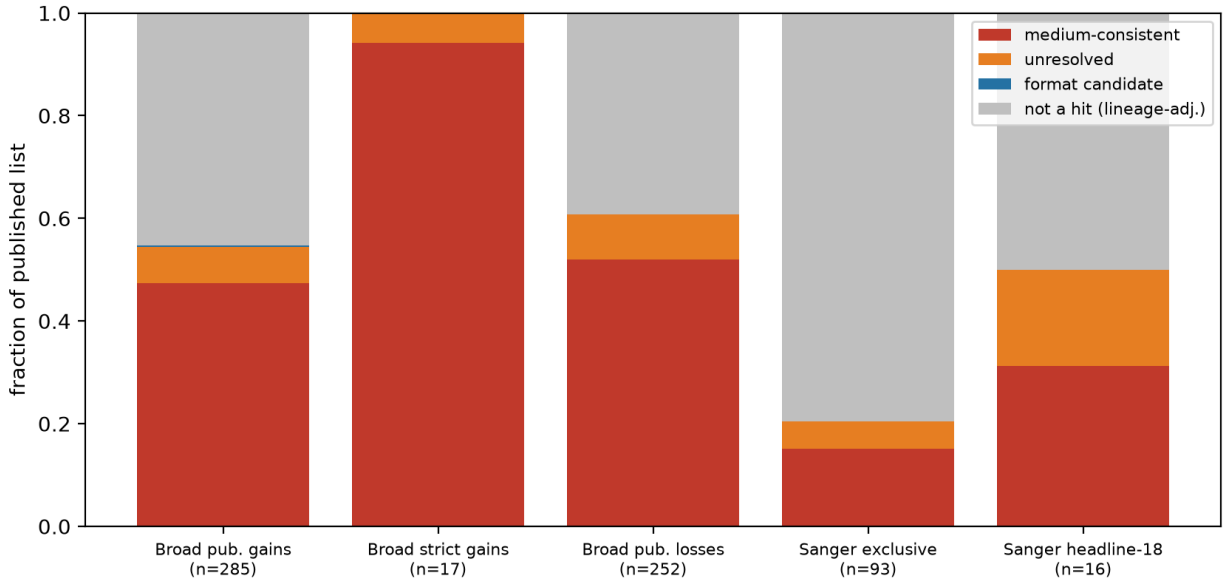


Figure 3. Flag composition of published organoid-specific hit lists (Broad figshare table; Herranz-Ors supplementary table 4).

Supplementary data: per-gene attribution tables (raw and normalized), held-out contrasts, survivor candidates, and analysis code accompany this preprint (release bundle v1). Inputs: DepMap 26Q3 (portal), Broad NextGen figshare (doi:10.6084/m9.figshare.29472362), Sanger figshare supplementary tables, Rossiter et al. 2021 Table S1 (PMC8172426).